

Rate-Region Characterization and Channel Estimation for Cell-Free Symbiotic Radio Communications

Zhuoyin Dai, Ruoguang Li, Jingran Xu, Yong Zeng, *Member, IEEE*, and Shi Jin, *Senior Member, IEEE*

Abstract—Cell-free massive MIMO and symbiotic radio communication have been recently proposed as the promising beyond fifth-generation (B5G) networking architecture and transmission technology, respectively. To reap the benefits of both, this paper studies cell-free symbiotic radio communication systems, where a number of cell-free access points (APs) cooperatively send primary information to a receiver, and simultaneously support the passive backscattering communication of the secondary backscatter device (BD). We first derive the achievable communication rates of the active primary user and passive secondary user under the assumption of perfect channel state information (CSI), based on which the transmit beamforming of the cell-free APs is optimized to characterize the achievable rate-region of cell-free symbiotic communication systems. Furthermore, to practically acquire the CSI of the active and passive channels, we propose an efficient channel estimation method based on two-phase uplink-training, and the achievable rate-region taking into account CSI estimation errors are further characterized. Simulation results are provided to show the effectiveness of our proposed beamforming and channel estimation methods.

Index Terms—cell-free massive MIMO, symbiotic radio, backscattering, channel estimation, active and passive communication.

I. INTRODUCTION

With the ongoing commercial deployment of the fifth-generation (5G) mobile communication networks, the academia and industry communities have started the investigation of the key technologies for beyond fifth-generation (B5G) or the sixth-generation (6G) networks [1]–[3]. In order to meet the orders-of-magnitude performance improvement in terms of coverage, connectivity density, data rate, reliability, latency, etc., many promising technologies are being investigated, such as extremely large-scale MIMO/surface [4], [5], millimeter wave or TeraHertz communication [6], [7], non-terrestrial networks (NTN) [8], [9], reconfigurable intelligent surface (RIS) [10], [11], and artificial intelligence (AI)-aided wireless communications [12]. On the other hand, *cell-free massive MIMO* [13] and *symbiotic radio communication* [14] were recently proposed as the promising B5G networking architecture and transmission technology, respectively, which have received fast-growing attentions.

This work was supported by the National Key R&D Program of China with grant number 2019YFB1803400. Part of this work has been presented at the 2021 IEEE/CIC ICC Workshops, Xiamen, China, 28-30 Jul. 2021 [15].

The authors are with the National Mobile Communications Research Laboratory, Southeast University, Nanjing 210096, China. Y. Zeng is also with the Purple Mountain Laboratories, Nanjing 211111, China (e-mail: {zhuoyin_dai, ruoguangli, jingran_xu, yong_zeng, jinshi}@seu.edu.cn). (*Corresponding author: Yong Zeng.*)

As a radically new potential networking architecture for B5G mobile communication networks, cell-free massive MIMO is significantly different from the classical cellular architecture since it blurs the conventional concepts of cells or cell boundaries [13]. Instead, geographically distributed access points (APs) [16], [17], which are connected to the central processing unit (CPU), cooperatively serve their surrounding users to achieve high macro diversity. Cell-free massive MIMO is expected to mitigate the inter-cell interference issues suffered by small cell systems and provide users with consistently high quality of service everywhere [18]. Significant research efforts have been recently devoted to the theoretical study and practical design of cell-free massive MIMO systems. For example, the performance of two basic linear precoding schemes, i.e., conjugate beamforming and zero-forcing precoding, was compared for cell-free massive MIMO in [19]. The receiver filter coefficients and power allocation of cell-free massive MIMO were optimized to maximize the minimal user rate or bandwidth efficiency in [20], [21]. Furthermore, in [22], [23], the communication resource allocation was optimized to maximize the energy efficiency and spectral efficiency of cell-free massive MIMO systems.

On the other hand, symbiotic radio has been recently proposed as a promising B5G transmission technology [14], which is able to exploit the benefits of the conventional cognitive radio (CR) and the emerging passive ambient backscattering communications (AmBC) to realize spectral- and energy-efficient communications [24]. Specifically, the passive secondary backscatter device (BD) in symbiotic radio systems reuses not only the spectrum of the active primary communication as in traditional CR systems, but also its power via passive backscattering technology [25]. Based on the relationship of symbol durations of the primary and secondary signals, symbiotic radio systems can be classified as *commensal symbiotic radio* (CSR) and *parasite symbiotic radio* (PSR) [26]. In CSR, the secondary signals have much longer symbol durations than the primary signals, rendering the secondary backscattering communication to contribute additional multipath components to enhance the primary communication. As a result, the primary and secondary communications form a mutualism relationship [24]. On the other hand, for PSR, the primary and secondary signals have equal symbol durations, so that the secondary signals may interfere with the primary signal. However, compared to the CSR case, the secondary communication rate in PSR can be significantly improved. Significant research efforts have been devoted to the study

of symbiotic radio systems. For example, in order to maximize the secondary communication rate, an exact penalty beamforming method based on the local optimal solution was proposed in [27]. Besides, [28] and [29] investigated how to effectively allocate communication resources such as transmit power and reflection coefficient, so as to improve the energy efficiency and achievable rates of symbiotic radio.

It is worth remarking that all the aforementioned existing works studied cell-free massive MIMO or symbiotic radio communication systems separately, i.e., cell-free systems with conventional active communication or symbiotic radio transmission in conventional cellular network or the simplest point-to-point communications. As the promising B5G networking architecture and transmission technology, respectively, it is natural that cell-free networking and symbiotic radio communication would merge into each other to reap the benefits of both. This motivates our current work to investigate cell-free symbiotic radio communication systems, which, to the best of our knowledge, have not been studied in the existing literature. By combining cell-free architecture with symbiotic radio transmission technology, the passive secondary communication in symbiotic radio system is enhanced by the cooperation gain of distributed APs, thus realizing passive communication with high macro-diversity. In this paper, we study a basic cell-free symbiotic radio system, in which a number of distributed multi-antenna APs cooperatively send primary information to a receiver, and concurrently support the passive backscattering communication of the secondary BD. As such, the distributed cooperation gain by APs can be exploited to enhance both the primary and secondary communication rates. Our specific contributions are summarized as follows:

- First, we present the mathematical model of cell-free symbiotic radio communication systems, which is a promising system that exploits both advantages of cell-free networking architecture and symbiotic radio transmission technology. Under the assumption of perfect channel state information (CSI) of the direct active channels and cascaded passive channels, the achievable rates of both the primary and secondary communications are derived.
- Next, we relax the assumption of perfect CSI and investigate the practical CSI acquisition method for the considered cell-free symbiotic radio system. Similar to the extensively studied massive MIMO systems, efficient channel estimation for cell-free massive MIMO can be achieved by exploiting the uplink-downlink channel reciprocity [30]–[32], i.e., the downlink channels can be efficiently estimated via uplink training. However, different from the existing cell-free massive MIMO systems [13], the channel estimation for cell-free symbiotic radio system requires estimating not only the active direct-link channels, but also the passive backscatter channels. To this end, we propose a two-phase based channel estimation method for cell-free symbiotic radio communication systems. In the first phase, pilot symbols are sent by the receiver while muting the BD, so as to estimate the direct-link channels. In the second phase, pilots are

sent by both the receiver and the BD so that, together with the estimation of the direct-link channels, the cascaded backscatter channels are estimated. Furthermore, the channel estimation errors in both phases are derived, which are shown to be dependent on the total pilot length and the pilot allocation between the two training phases. The achievable rates under imperfect CSI are derived by taking into account the CSI estimation errors.

- Furthermore, for both the ideal scenario with perfect CSI and practical scenario of imperfect CSI with channel estimation errors, we formulate the beamforming optimization problem to characterize the achievable rate-region of the active primary communication and the passive secondary communication. The formulated problems are non-convex in general, which are difficult to be directly solved. We show that a closed-form solution can be obtained for the special case when the targeting primary rate is relatively small. Furthermore, for the general cases, we show that the rate threshold constraint can be converted into the convex second-order cone (SOC) constraint, and that the nonconcave objective function can be globally lower-bounded by its first-order Taylor expansion. Therefore, efficient algorithms are proposed based on successive convex approximation (SCA) technique [33]–[35]. Numerical results are provided to demonstrate that the proposed channel estimation and optimization approaches are effective in cell-free symbiotic radio communication systems.

The rest of this paper is organized as follows. Section II presents the mathematical model of cell-free symbiotic radio communication systems. Under the assumption of perfect CSI, Section III characterizes the achievable rate-region of passive secondary communication and active primary communication by optimizing the transmit beamforming of the APs. In Section IV, a two-phase uplink-training based channel estimation method is proposed, and the achievable primary and secondary communication rates taking into account the channel estimation errors are derived. Furthermore, the beamforming optimization problem with imperfect CSI is also studied in Section IV. Section V presents numerical results to validate our proposed designs. Finally, we conclude the paper in Section VI.

Notations: In this paper, scalars are denoted by italic letters. Vectors and matrices are denoted by boldface lower- and upper-case letters respectively. $\mathbb{C}^{N \times 1}$ denotes the space of N -dimensional complex-valued vectors. $\text{Re}\{\cdot\}$ and $\text{Im}\{\cdot\}$ denote the real and imaginary parts, respectively. $\mathbb{E}_X[\cdot]$ denotes the expectation with respect to the random variable X . $\text{Ei}(x) \triangleq \int_{-\infty}^x \frac{1}{u} e^u du$ denotes the exponential integral from $-\infty$ to x . \mathbf{I}_N denotes an $N \times N$ identity matrix. For a vector \mathbf{a} , its transpose, Hermitian transpose, and Euclidean norm are respectively denoted as \mathbf{a}^T , \mathbf{a}^H and $\|\mathbf{a}\|$. Meanwhile, $\mathbf{a}[m : m + n]$ represents the subvector of \mathbf{a} made up of its m th to $(m + n)$ -th elements. $\log_2(\cdot)$ denotes the logarithm with base 2. Furthermore, $\mathcal{CN}(\mu, \sigma^2)$ denotes the circularly symmetric complex Gaussian (CSCG) distribution with mean μ and variance σ^2 .

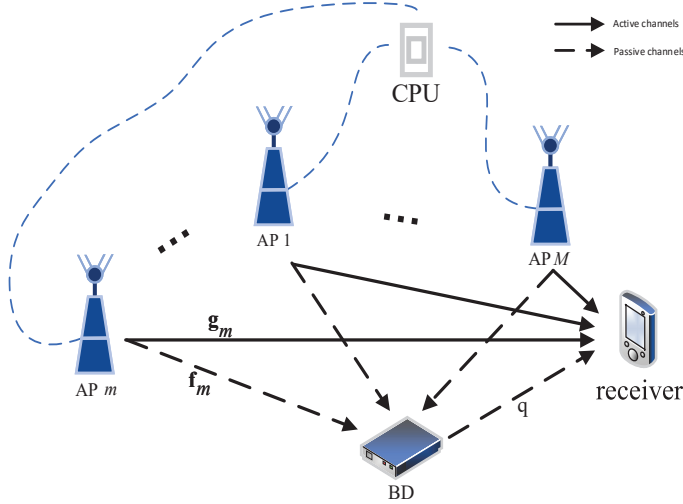


Fig. 1. Cell-free symbiotic radio communication system, where M distributed APs cooperatively transmit primary information to the receiver and concurrently support the secondary passive backscattering communication.

II. SYSTEM MODEL

As shown in Fig. 1, we consider a cell-free symbiotic radio system, which consists of M distributed APs, one information receiver, and one BD. The M APs cooperatively send primary information to the receiver, and simultaneously support the BD for secondary communication via passive backscattering to the same information receiver. The considered system may model a wide range of applications, e.g., with the receiver corresponding to smartphones and the BD being the smart home sensor node. We assume that each AP is equipped with N antennas, whereas the receiver and BD each has one antenna. Denote by $\mathbf{g}_m \in \mathbb{C}^{N \times 1}$ and $\mathbf{f}_m \in \mathbb{C}^{N \times 1}$ the multiple-input single-output (MISO) channels from the m th AP to the receiver and BD, respectively, where $m = 1, \dots, M$. Further denote by $q \in \mathbb{C}$ the channel coefficient from the BD to the receiver. Thus, the cascaded backscatter channel from the m th AP to the receiver via the BD is $q\mathbf{f}_m$.

In this paper, we focus on the PSR setup [24], where the symbol durations of the primary and secondary signals are equal. Let $s(n) \sim \mathcal{CN}(0, 1)$ and $c(n) \sim \mathcal{CN}(0, 1)$ denote the CSCG information-bearing symbols of the primary and secondary signals, respectively. Further denote by $\mathbf{w}_m \in \mathbb{C}^{N \times 1}$ the transmit beamforming vector of the m th AP, where its power is $\|\mathbf{w}_m\|^2 \leq P_m$, with P_m denoting the maximum allowable transmit power of the m th AP. The received signal by the receiver is

$$r(n) = \sum_{m=1}^M [\mathbf{g}_m^H \mathbf{w}_m s(n) + \sqrt{\alpha} q \mathbf{f}_m^H \mathbf{w}_m s(n) c(n)] + z(n), \quad (1)$$

where α denotes the power reflection coefficient of the BD, $z(n) \sim \mathcal{CN}(0, \sigma^2)$ is the additive white Gaussian noise (AWGN). Based on the received signal $r(n)$ in (1), the receiver needs to decode both the primary and secondary signals. Since the backscatter link is typically much weaker than the direct link, the receiver may first decode the primary symbols $s(n)$, by treating the backscatter interfering signals

as noise, whose power is $\mathbb{E}[|\sqrt{\alpha} \sum_{m=1}^M q \mathbf{f}_m^H \mathbf{w}_m s(n) c(n)|^2] = \alpha |q|^2 |\sum_{m=1}^M \mathbf{f}_m^H \mathbf{w}_m|^2$. Therefore, the signal-to-interference-plus-noise ratio (SINR) for decoding the primary information is

$$\gamma_s = \frac{|\sum_{m=1}^M \mathbf{g}_m^H \mathbf{w}_m|^2}{\alpha |q|^2 |\sum_{m=1}^M \mathbf{f}_m^H \mathbf{w}_m|^2 + \sigma^2}. \quad (2)$$

Note that due to the product of $c(n)$ and $s(n)$ in the second term of (1), the resulting noise for decoding $s(n)$ no longer follows Gaussian distribution. However, by using the fact that for any given noise power, Gaussian noise results in the maximum entropy and hence constitutes the worst-case noise [36], [37], the achievable rate of the primary communication in (1) is

$$R_s = \log_2(1 + \gamma_s). \quad (3)$$

After decoding the primary information, the first term in (1) can be subtracted from the received signal before decoding the secondary symbols $c(n)$. The resulting signal is

$$\hat{r}_c(n) = \sqrt{\alpha} q \sum_{m=1}^M \mathbf{f}_m^H \mathbf{w}_m s(n) c(n) + z(n). \quad (4)$$

Note that since $s(n)$ varies across different secondary symbols $c(n)$, (4) can be interpreted as a fast-fading channel, whose instantaneous channel gain depends on $|s(n)|^2$ [38]. With $s(n) \sim \mathcal{CN}(0, 1)$, its squared envelope follows an exponential distribution. Therefore, the ergodic rate of the backscattering communication (4) can be expressed as [24], [39]

$$\begin{aligned} R_c &= \mathbb{E}_{s(n)} \left[\log_2 \left(1 + \frac{\alpha |q|^2 |\sum_{m=1}^M \mathbf{f}_m^H \mathbf{w}_m|^2 |s(n)|^2}{\sigma^2} \right) \right] \\ &= \int_0^\infty \log_2(1 + \beta_c x) e^{-x} dx \\ &= -e^{-\frac{1}{\beta_c}} \text{Ei} \left(-\frac{1}{\beta_c} \right) \log_2 e, \end{aligned} \quad (5)$$

where $\text{Ei}(-\frac{1}{\beta_c})$ is the exponential integral, and $\beta_c = \frac{\alpha |q|^2 |\sum_{m=1}^M \mathbf{f}_m^H \mathbf{w}_m|^2}{\sigma^2}$ is the average received signal-to-noise ratio (SNR) of the backscatter link.

III. RATE-REGION CHARACTERIZATION WITH PERFECT CSI

In this section, under the assumption that perfect CSI is available at the APs, we aim to characterize the achievable rate-region of the active primary communication and passive secondary communication, by optimizing the transmit beamforming of the M APs. To this end, the beamforming optimization problem is formulated to maximize the ergodic rate of the backscattering communication in (5), subject to a given targeting communication rate constraint for the primary communication. By varying the targeting communication rate, the complete Pareto boundary of the achievable communication rate-region can be obtained. The problem can be formulated as

$$\max_{\mathbf{w}_m, m=1, \dots, M} R_c \quad (6a)$$

$$\text{s.t. } R_s \geq R_{\text{th}}, \quad (6b)$$

$$\|\mathbf{w}_m\|^2 \leq P_m, \quad m = 1, \dots, M, \quad (6c)$$

where R_{th} denotes the given targeting threshold for the primary communication rate, and (6c) corresponds to the per-AP power constraint.

It has been shown in [24] that the first-order derivative of the ergodic rate R_c in (5) with respect to the average received SNR β_c is non-negative. Therefore, R_c is a monotonically non-decreasing function with respect to β_c . Thus, we may replace the objective function of (6) by β_c . By further ignoring those constant terms, problem (6) can be equivalently written as

$$\max_{\mathbf{w}} |\mathbf{f}^H \mathbf{w}|^2 \quad (7a)$$

$$\text{s.t. } \log_2 \left(1 + \frac{|\mathbf{g}^H \mathbf{w}|^2}{\alpha|q|^2|\mathbf{f}^H \mathbf{w}|^2 + \sigma^2} \right) \geq R_{\text{th}}, \quad (7b)$$

$$\|\mathbf{w}[(m-1)N+1:mN]\|^2 \leq P_m, \quad m = 1, \dots, M, \quad (7c)$$

where we have defined the cascaded vectors as $\mathbf{g}^T = [\mathbf{g}_1^T, \mathbf{g}_2^T, \dots, \mathbf{g}_M^T]$, $\mathbf{f}^T = [\mathbf{f}_1^T, \mathbf{f}_2^T, \dots, \mathbf{f}_M^T]$ and $\mathbf{w}^T = [\mathbf{w}_1^T, \mathbf{w}_2^T, \dots, \mathbf{w}_M^T]$.

Before solving problem (7), we first study its feasibility property. Obviously, problem (7) will become infeasible if R_{th} is too large. It is not difficult to see that problem (7) is feasible if and only if $R_{\text{th}} \leq \bar{R}_s$, where \bar{R}_s is the optimal value to the following optimization problem

$$\max_{\mathbf{w}} \log_2 \left(1 + \frac{|\mathbf{g}^H \mathbf{w}|^2}{\alpha|q|^2|\mathbf{f}^H \mathbf{w}|^2 + \sigma^2} \right) \quad (8a)$$

$$\text{s.t. } \|\mathbf{w}[(m-1)N+1:mN]\|^2 \leq P_m, \quad m = 1, \dots, M. \quad (8b)$$

Next, we consider solving problem (8) to get the maximum achievable primary communication rate threshold \bar{R}_s for problem (7) to be feasible. Note that the objective function of problem (8) is nonconcave with respect to \mathbf{w} . Thus, problem (8) cannot be efficiently solved directly with standard convex optimization technique. Fortunately, the efficient optimal solution can be obtained via bisection method with convex optimization. To this end, it is not difficult to see that if \mathbf{w}^* is an optimal solution to problem (8), so is $\mathbf{w}^*e^{j\phi}$ for any phase rotation ϕ . This is because any arbitrary phase rotation for the beamforming vector \mathbf{w}^* does not change the objective function in (8a) nor the constraint in (8b). Therefore, without loss of optimality to problem (8), we may assume that $\mathbf{g}^H \mathbf{w}$ is a nonnegative real number, i.e., $\text{Re}\{\mathbf{g}^H \mathbf{w}\} \geq 0$, and $\text{Im}\{\mathbf{g}^H \mathbf{w}\} = 0$. As a result, by further introducing a slack variable μ , problem (8) can be equivalently written as

$$\max_{\mathbf{w}} \mu \quad (9a)$$

$$\text{s.t. } \log_2 \left(1 + \frac{(\text{Re}\{\mathbf{g}^H \mathbf{w}\})^2}{\alpha|q|^2|\mathbf{f}^H \mathbf{w}|^2 + \sigma^2} \right) \geq \mu, \quad (9b)$$

$$\|\mathbf{w}[(m-1)N+1:mN]\|^2 \leq P_m, \quad m = 1, \dots, M, \quad (9c)$$

$$\text{Im}\{\mathbf{g}^H \mathbf{w}\} = 0. \quad (9d)$$

Furthermore, for any given μ , we may formulate the following feasibility problem

$$\text{Find } \mathbf{w} \quad (10a)$$

$$\text{s.t. } \|\sigma, \sqrt{\alpha}q\mathbf{f}^H \mathbf{w}\|_2 \leq \frac{\text{Re}\{\mathbf{g}^H \mathbf{w}\}}{\sqrt{2^\mu - 1}}, \quad (10b)$$

$$\|\mathbf{w}[(m-1)N+1:mN]\|^2 \leq P_m, \quad m = 1, \dots, M, \quad (10c)$$

$$\text{Im}\{\mathbf{g}^H \mathbf{w}\} = 0. \quad (10d)$$

Note that (10b) is equivalent to (9b), which is expressed as an SOC constraint for any given μ . Thus, problem (10) is a SOC programming (SOCP) problem, which can be efficiently solved by standard convex optimization technique or existing software tools such as CVX [40]. If problem (10) is feasible, then the optimal value \bar{R}_s of (8) satisfies $\bar{R}_s \geq \mu$; otherwise, $\bar{R}_s < \mu$. As a result, the optimal solution to problem (8) can be obtained by solving the SOCP feasibility problem (10), together with the efficient bisection method to update μ , which is summarized in Algorithm 1.

After obtaining \bar{R}_s by optimally solving the optimization problem (8) with Algorithm 1, we consider the optimization problem (7) for any given rate threshold $R_{\text{th}} \leq \bar{R}_s$, so that (7) is guaranteed to be feasible. We first show that when R_{th} is small enough, the optimal solution to problem (7) can be obtained in closed-form, which is stated in the following Theorem.

Theorem 1. When $R_{\text{th}} \leq \hat{R}_s$, where

$$\hat{R}_s \triangleq \log_2 \left(1 + \frac{|\sum_{m=1}^M \sqrt{P_m} \frac{\mathbf{g}_m^H \mathbf{f}_m}{\|\mathbf{f}_m\|}|^2}{\alpha|q|^2 |\sum_{m=1}^M \sqrt{P_m} \|\mathbf{f}_m\| |^2 + \sigma^2} \right), \quad (11)$$

the optimal solution and optimal objective value to problem (7) can be obtained in closed-form as

$$\mathbf{w}_m^* = \sqrt{P_m} \frac{\mathbf{f}_m}{\|\mathbf{f}_m\|}, \quad m = 1, \dots, M, \quad (12)$$

$$|\mathbf{f}^H \mathbf{w}^*|^2 = \left(\sum_{m=1}^M \sqrt{P_m} \|\mathbf{f}_m\| \right)^2. \quad (13)$$

Proof. Please refer to Appendix A. ■

Under the condition of Theorem 1 and with the closed-form optimal solution to problem (7) given in (12), the resulting primary communication rate \hat{R}_s is given in (11). Furthermore,

Algorithm 1 Optimal solution to problem (8)

Input: The channel coefficients $q\mathbf{f}$ and \mathbf{h} , noise power σ^2 , power reflection coefficient α , termination threshold κ_1 , maximum transmit power $P_m, m = 1, \dots, M$.

Output: The optimal solution \mathbf{w}^* and the maximum primary communication rate \bar{R}_s to problem (8).

- 1: Initialization: $\mu_{\min} = 0$, and μ_{\max} to a sufficiently large value.
- 2: **while** $\mu_{\max} - \mu_{\min} > \kappa_1 \mu_{\min}$ **do**
- 3: $\mu = \frac{\mu_{\min} + \mu_{\max}}{2}$.
- 4: For the given μ , solve the feasibility problem (10).
- 5: **if** problem (10) is feasible and let \mathbf{w}^* denote its solution, **then**
- 6: $\mu_{\min} = \mu, \bar{R}_s = \mu, \mathbf{w}^* = \mathbf{w}^*$.
- 7: **else**
- 8: $\mu_{\max} = \mu$.
- 9: **end if**
- 10: **end while**
- 11: Output \bar{R}_s and \mathbf{w}^* .

by substituting (13) into (5), the secondary communication rate \hat{R}_c is obtained in closed-form as

$$\hat{R}_c = -e^{\frac{1}{\beta_c}} \text{Ei}\left(-\frac{1}{\beta_c}\right) \log_2 e, \quad (14)$$

where $\hat{\beta}_c = \frac{\alpha|q|^2 \left| \sum_{m=1}^M \sqrt{P_m} \|\mathbf{f}_m\| \right|^2}{\sigma^2}$ is the average received SNR of the backscatter link.

With the above discussions, the remaining task for solving problem (7) is to consider the case $\hat{R}_s < R_{\text{th}} \leq \bar{R}_s$. In this case, due to the non-concave objective function (7a) and the nonconvex constraint (7b), problem (7) is non-convex. Thus, it is difficult to find the optimal solution efficiently. Fortunately, an efficient Karush–Kuhn–Tucker (KKT) local optimal solution can be obtained by using the SCA technique. Towards this end, it is first observed that similar to (10b), without loss of optimality, the rate constraint in (7b) can be written as a SOC constraint. Thus, problem (7) can be equivalently written as

$$\max_{\mathbf{w}} \quad |\mathbf{f}^H \mathbf{w}|^2 \quad (15a)$$

$$\text{s.t.} \quad \left\| [\sigma, \sqrt{\alpha} q \mathbf{f}^H \mathbf{w}] \right\|_2 \leq \frac{\text{Re}\{\mathbf{g}^H \mathbf{w}\}}{\sqrt{2R_{\text{th}} - 1}}, \quad (15b)$$

$$\left\| \mathbf{w}[(m-1)N + 1 : mN] \right\|^2 \leq P_m, \quad m = 1, \dots, M, \quad (15c)$$

$$\text{Im}\{\mathbf{g}^H \mathbf{w}\} = 0. \quad (15d)$$

Problem (15) is still non-convex as the objective function (15a) is a convex function with respect to \mathbf{w} , the maximization of which is a non-convex optimization problem. To address this issue, the SCA technique is applied to find a KKT local optimal solution iteratively [33]–[35]. Specifically, consider the current iteration l , in which the local point $\{\mathbf{w}^{(l)}\}$ is obtained in the previous iteration. Define $F(\mathbf{w}) = |\mathbf{f}^H \mathbf{w}|^2$, which is a convex differentiable function with respect to \mathbf{w} .

Algorithm 2 SCA for problem (15)

Input: The channel coefficients $q\mathbf{f}$ and \mathbf{h} , noise power σ^2 , power reflection coefficient α , maximum transmit power $P_m, m = 1, \dots, M$, rate threshold R_{th} and termination threshold κ_2 .

Output: The beamforming solution \mathbf{w}^* .

- 1: Initialization: set the iteration number $l = 0$, and initialize $\mathbf{w}^{(0)}$, so that it is feasible to (15).
- 2: **repeat**
- 3: For the given local point $\mathbf{w}^{(l)}$, solve the convex optimization problem (17) and denote the optimal solution as $\mathbf{w}^{*(l)}$.
- 4: Update the local point with $\mathbf{w}^{(l+1)} = \mathbf{w}^{*(l)}$.
- 5: Update $l = l + 1$,
- 6: **until** the fractional increase of the objective value of (15) is below the threshold κ_2 .

By using the fact that the first-order Taylor expansion of a convex differentiable function provides a global lower bound [41], [42], we have

$$\begin{aligned} F(\mathbf{w}) &\geq F(\mathbf{w}^{(l)}) + 2\text{Re}\left\{\mathbf{w}^{(l)H} \mathbf{f} \mathbf{f}^H (\mathbf{w} - \mathbf{w}^{(l)})\right\} \\ &\triangleq F_{\text{low}}(\mathbf{w}|\mathbf{w}^{(l)}), \forall \mathbf{w}. \end{aligned} \quad (16)$$

Therefore, by replacing the objective function in (15a) with its global lower bound in (16), we have the following optimization problem

$$\max_{\mathbf{w}} \quad |\mathbf{f}^H \mathbf{w}^{(l)}|^2 + 2\text{Re}\left\{\mathbf{w}^{(l)H} \mathbf{f} \mathbf{f}^H (\mathbf{w} - \mathbf{w}^{(l)})\right\} \quad (17a)$$

$$\text{s.t.} \quad \left\| [\sigma, \sqrt{\alpha} q \mathbf{f}^H \mathbf{w}] \right\|_2 \leq \frac{\text{Re}\{\mathbf{g}^H \mathbf{w}\}}{\sqrt{2R_{\text{th}} - 1}}, \quad (17b)$$

$$\left\| \mathbf{w}[(m-1)N + 1 : mN] \right\|^2 \leq P_m, \quad m = 1, \dots, M, \quad (17c)$$

$$\text{Im}\{\mathbf{g}^H \mathbf{w}\} = 0. \quad (17d)$$

For any given local point $\mathbf{w}^{(l)}$, the objective function of (17a) is a concave affine function of the optimization variable \mathbf{w} , and all constraints are convex. Therefore, problem (17) is a convex optimization problem, which can be efficiently solved with standard convex optimization techniques or readily available software toolboxes, such as CVX [40]. Thanks to the global lower bound in (16), the optimal objective value of the convex optimization problem (17) provides at least a lower bound to that of the non-convex optimization problem (15). By successively updating the local point $\mathbf{w}^{(l)}$ and solving (17), a monotonically non-decreasing objective value of (15) can be obtained. The algorithm is summarized in Algorithm 2.

Let $F(\mathbf{w}^{*(l)}) = |\mathbf{f}^H \mathbf{w}^{*(l)}|^2$ denote the objective value of problem (15) with the beamforming vector obtained during the (l) -th iteration of Algorithm 2. We have the following Lemma:

Lemma 1. The value $F(\mathbf{w}^{*(l)})$ obtained during each iteration of Algorithm 2 is monotonically non-decreasing, i.e., $F(\mathbf{w}^{*(l+1)}) \geq F(\mathbf{w}^{*(l)}), \forall l$. Besides, the sequence

$\{\mathbf{w}^{*(l)}\}, l = 1, 2, \dots$, converges to a KKT solution of the original non-convex problem (15).

Proof. Please refer to Appendix B. ■

IV. CHANNEL ESTIMATION AND RATE-REGION CHARACTERIZATION WITH IMPERFECT CSI

Note that the above analysis is based on the assumption of perfect CSI on $\mathbf{f}_m, \mathbf{g}_m, m = 1, \dots, M$, and q . In practical wireless communication systems, these channels need to be acquired via e.g., pilot-based channel estimation. In the following, we propose an efficient channel estimation method for cell-free symbiotic radio systems based on two-phase uplink training. Furthermore, the achievable rates taking into account the channel estimation errors are derived, and the beamforming optimization problem is revisited with imperfect CSI to characterize the achievable rate-region with imperfect CSI.

In the first phase of the proposed channel estimation method, pilot symbols are sent by the receiver while the BD is muted, so as to estimate the direct-link channels $\mathbf{g}_m, m = 1, \dots, M$. In the second phase, pilots are sent both by the receiver and the BD, so that, together with the estimation of the direct-link channels \mathbf{g}_m , the cascaded backscatter channels $q\mathbf{f}_m$, are estimated. The details are elaborated in the following.

A. Direct-Link Channel Estimation

First, we discuss the uplink training-based estimation of the direct-link channels between the receiver and the M APs. Denote by τ_1 the length of the uplink training sequence, and let P_t be the training power. Further denote by $\boldsymbol{\varphi}_1 \in \mathbb{C}^{\tau_1 \times 1}$ the pilot sequence, where $\|\boldsymbol{\varphi}_1\|^2 = \tau_1$. The received training signals by N antennas of the m th AP over the τ_1 symbol durations, which is denoted as $\mathbf{Y}'_m \in \mathbb{C}^{N \times \tau_1}$, can be written as

$$\mathbf{Y}'_m = \sqrt{P_t} \mathbf{g}_m \boldsymbol{\varphi}_1^H + \mathbf{Z}'_m, \quad m = 1, \dots, M, \quad (18)$$

where \mathbf{Z}'_m denotes the i.i.d. CSCG noise with zero-mean and power σ^2 . With the pilot sequence $\boldsymbol{\varphi}_1$ known at the APs, \mathbf{Y}'_m can be projected to $\boldsymbol{\varphi}_1$, which gives

$$\check{\mathbf{y}}'_m = \frac{1}{\sqrt{P_t}} \mathbf{Y}'_m \boldsymbol{\varphi}_1 = \tau_1 \mathbf{g}_m + \frac{1}{\sqrt{P_t}} \hat{\mathbf{z}}'_m, \quad (19)$$

where $\hat{\mathbf{z}}'_m \triangleq \mathbf{Z}'_m \boldsymbol{\varphi}_1$ is the resulting noise vector. It can be shown that $\hat{\mathbf{z}}'_m$ is i.i.d. CSCG noise with power $\tau_1 \sigma^2$, i.e., $\hat{\mathbf{z}}'_m \sim \mathcal{CN}(\mathbf{0}, \tau_1 \sigma^2 \mathbf{I}_N)$.

With \mathbf{g}_m being a zero-mean random vector, its linear minimum mean square error estimation (LMMSE), denoted by $\hat{\mathbf{g}}_m \in \mathbb{C}^{N \times 1}$, is [43]

$$\begin{aligned} \hat{\mathbf{g}}_m &= \mathbb{E}[\mathbf{g}_m \check{\mathbf{y}}_m'^H] (\mathbb{E}[\check{\mathbf{y}}_m' \check{\mathbf{y}}_m'^H])^{-1} \check{\mathbf{y}}_m' \\ &= \mathbf{R}_{\mathbf{g},m} (\tau_1 \mathbf{R}_{\mathbf{g},m} + \frac{\sigma^2}{P_t} \mathbf{I}_N)^{-1} \check{\mathbf{y}}_m', \end{aligned} \quad (20)$$

where $\mathbf{R}_{\mathbf{g},m} = \mathbb{E}[\mathbf{g}_m \mathbf{g}_m^H]$ denotes the covariance matrix of \mathbf{g}_m . By further decomposing the direct-link channel as $\mathbf{g}_m =$

$\sqrt{b_m} \mathbf{d}_m$, with b_m denoting the large-scale channel coefficient, and $\mathbf{d}_m \in \mathbb{C}^{N \times 1}$ denoting the zero-mean CSCG small-scale fading component, i.e., $\mathbf{d}_m \sim \mathcal{CN}(\mathbf{0}, \mathbf{I}_N)$. Then \mathbf{g}_m is CSCG distributed with covariance matrix $\mathbf{R}_{\mathbf{g},m} = b_m \mathbf{I}_N$, and thus LMMSE estimation is also the optimal MMSE estimation. In this case, (20) can be simplified as

$$\hat{\mathbf{g}}_m = \frac{P_t b_m}{P_t \tau_1 b_m + \sigma^2} \check{\mathbf{y}}_m'. \quad (21)$$

It can be shown that $\hat{\mathbf{g}}_m$ follows the distribution

$$\hat{\mathbf{g}}_m \sim \mathcal{CN}(\mathbf{0}, \frac{e_1 b_m^2}{1 + e_1 b_m} \mathbf{I}_N), \quad (22)$$

where we have defined the transmit training energy-to-noise ratio (ENR) as $e_1 \triangleq \frac{P_t \tau_1}{\sigma^2}$.

Let $\tilde{\mathbf{g}}_m$ denote the channel estimation error of the m th AP, i.e., $\tilde{\mathbf{g}}_m = \mathbf{g}_m - \hat{\mathbf{g}}_m$. With MMSE estimation, it is known that $\tilde{\mathbf{g}}_m$ is uncorrelated with $\hat{\mathbf{g}}_m$ [43], which follows the distribution

$$\tilde{\mathbf{g}}_m \sim \mathcal{CN}(\mathbf{0}, \frac{b_m}{1 + e_1 b_m} \mathbf{I}_N). \quad (23)$$

It is observed from (23) that as the transmit training ENR e_1 increases, the variance of the channel estimation error reduces, as expected.

B. Backscatter Channel Estimation

With the estimation $\hat{\mathbf{g}}_m$ for the direct-link channels obtained in the first phase, in the second phase, pilot symbols are sent from both the receiver and the BD to estimate the cascaded passive backscatter channels $q\mathbf{f}_m, m = 1, \dots, M$. Let τ_2 denote the length of the training sequence in the second phase and $\boldsymbol{\varphi}_2 \in \mathbb{C}^{\tau_2 \times 1}$ be the pilot sequence sent by the receiver with $\|\boldsymbol{\varphi}_2\|^2 = \tau_2$. The received training signal by the m th AP can be written as

$$\mathbf{Y}_m^* = \sqrt{P_t \alpha} q \mathbf{f}_m \boldsymbol{\varphi}_2^H + \sqrt{P_t} (\hat{\mathbf{g}}_m + \tilde{\mathbf{g}}_m) \boldsymbol{\varphi}_2^H + \mathbf{Z}''_m, \quad (24)$$

where \mathbf{Z}''_m denotes the i.i.d. CSCG noise with power σ^2 . Note that without loss of generality, we assume that the pilot symbols backscattered by the BD are all equal to 1. After subtracting the terms related to the estimation $\hat{\mathbf{g}}_m$ of the direct-link channels from (24), we have

$$\mathbf{Y}''_m = \sqrt{P_t \alpha} q \mathbf{f}_m \boldsymbol{\varphi}_2^H + \sqrt{P_t} \tilde{\mathbf{g}}_m \boldsymbol{\varphi}_2^H + \mathbf{Z}''_m. \quad (25)$$

With $\boldsymbol{\varphi}_2$ known at the APs, the projection of \mathbf{Y}''_m after scaling by $\frac{1}{\sqrt{P_t \alpha}}$, is

$$\check{\mathbf{y}}''_m = \frac{1}{\sqrt{P_t \alpha}} \mathbf{Y}''_m \boldsymbol{\varphi}_2 = \tau_2 \mathbf{h}_m + \frac{\tau_2}{\sqrt{\alpha}} \tilde{\mathbf{g}}_m + \frac{1}{\sqrt{P_t \alpha}} \hat{\mathbf{z}}''_m, \quad (26)$$

where the cascaded backscatter channel is defined as $\mathbf{h}_m = q\mathbf{f}_m$, and $\hat{\mathbf{z}}''_m \triangleq \mathbf{Z}''_m \boldsymbol{\varphi}_2$. It can be shown that $\hat{\mathbf{z}}''_m \sim \mathcal{CN}(\mathbf{0}, \tau_2 \sigma^2 \mathbf{I}_N)$.

Let $\mathbf{R}_{\mathbf{h},m} = \mathbb{E}[\mathbf{h}_m \mathbf{h}_m^H]$ denote the covariance matrix of the cascaded backscatter channel \mathbf{h}_m . Then the LMMSE estimation of \mathbf{h}_m based on (26) is

$$\begin{aligned} \hat{\mathbf{h}}_m &= \mathbb{E}[\mathbf{h}_m \check{\mathbf{y}}_m''^H] (\mathbb{E}[\check{\mathbf{y}}_m'' \check{\mathbf{y}}_m''^H])^{-1} \check{\mathbf{y}}_m'' \\ &= \mathbf{R}_{\mathbf{h},m} (\tau_2 \mathbf{R}_{\mathbf{h},m} + \frac{\tau_2}{\alpha} \mathbf{R}_{\tilde{\mathbf{g}},m} + \frac{\sigma^2}{P_t \alpha} \mathbf{I}_N)^{-1} \check{\mathbf{y}}_m'', \end{aligned} \quad (27)$$

where $\mathbf{R}_{\tilde{\mathbf{g}}_m} = \mathbb{E}[\tilde{\mathbf{g}}_m \tilde{\mathbf{g}}_m^H]$ is the covariance matrix of $\tilde{\mathbf{g}}_m$.

If the channel coefficients in \mathbf{f}_m are i.i.d. distributed with variance ζ_m , we then have $\mathbf{R}_{\mathbf{h}_m} = \mathbb{E}[|q|^2 \mathbf{f}_m \mathbf{f}_m^H] = \epsilon_m \mathbf{I}_N$, where $\epsilon_m = \mathbb{E}[|q|^2] \zeta_m$.

Therefore, (27) can be simplified as

$$\hat{\mathbf{h}}_m = \frac{\alpha P_t \epsilon_m}{\alpha P_t \tau_2 \epsilon_m + \frac{P_t \tau_2 b_m}{1+e_1 b_m} + \sigma^2} \tilde{\mathbf{y}}_m'' \quad (28)$$

Define the transmit training ENR in the second phase as $e_2 \triangleq \frac{P_t \tau_2}{\sigma^2}$. Then with (23) and (28), we have

$$\mathbf{R}_{\hat{\mathbf{h}}_m} = \mathbb{E}[\hat{\mathbf{h}}_m \hat{\mathbf{h}}_m^H] = \frac{\alpha e_2 \epsilon_m^2}{\alpha e_2 \epsilon_m + \frac{e_2 b_m}{1+e_1 b_m} + 1} \mathbf{I}_N. \quad (29)$$

Let $\tilde{\mathbf{h}}_m = \mathbf{h}_m - \hat{\mathbf{h}}_m$ denote the estimation error. We have

$$\begin{aligned} \mathbf{R}_{\tilde{\mathbf{h}}_m} &\triangleq \mathbb{E}[(\mathbf{h}_m - \hat{\mathbf{h}}_m)(\mathbf{h}_m - \hat{\mathbf{h}}_m)^H] \\ &= \mathbf{R}_{\mathbf{h}_m} - \mathbf{R}_{\hat{\mathbf{h}}_m} \\ &= \frac{\epsilon_m (\frac{e_2 b_m}{1+e_1 b_m} + 1)}{\alpha e_2 \epsilon_m + \frac{e_2 b_m}{1+e_1 b_m} + 1} \mathbf{I}_N. \end{aligned} \quad (30)$$

It follows from (23) that if $e_1 \rightarrow \infty$, in which case the direct-link channel \mathbf{g}_m is perfectly estimated without any error, the variance of the estimation error in (30) reduces to the same form as that in (23).

C. Achievable Rate Analysis

In this subsection, we derive the achievable primary and secondary rates based on the channel estimation $\hat{\mathbf{g}}_m$ and $\hat{\mathbf{h}}_m$, $m = 1, \dots, M$, by taking into account the channel estimation errors. By substituting $\mathbf{g}_m = \hat{\mathbf{g}}_m + \tilde{\mathbf{g}}_m$ and $q\mathbf{f}_m = \hat{\mathbf{h}}_m + \tilde{\mathbf{h}}_m$ into (1), the received signal can be written as

$$r(n) = \sum_{m=1}^M [(\hat{\mathbf{g}}_m + \tilde{\mathbf{g}}_m)^H \mathbf{w}_m s(n) + \sqrt{\alpha} (\hat{\mathbf{h}}_m + \tilde{\mathbf{h}}_m)^H \mathbf{w}_m s(n) c(n)] + z(n). \quad (31)$$

For decoding the primary signals $s(n)$, besides the interference from the backscatter symbols $c(n)$, the term caused by the channel estimation error $\tilde{\mathbf{g}}_m$ is also treated as noise [37], [44]. Therefore, (31) can be decomposed as

$$r_s(n) = \text{DS}' \cdot s(n) + \text{ER} + \text{ST} + z(n), \quad (32)$$

where DS' , ER , and ST denote the desired signal, estimation errors and the secondary transmission signal, respectively, which are given by

$$\text{DS}' = \sum_{m=1}^M \hat{\mathbf{g}}_m^H \mathbf{w}_m, \quad (33)$$

$$\text{ER} = \sum_{m=1}^M (\tilde{\mathbf{g}}_m + \sqrt{\alpha} \tilde{\mathbf{h}}_m c(n))^H \mathbf{w}_m s(n), \quad (34)$$

$$\text{ST} = \sum_{m=1}^M \sqrt{\alpha} \hat{\mathbf{h}}_m^H \mathbf{w}_m s(n) c(n). \quad (35)$$

Therefore, the resulting SINR can be expressed as (36) shown at the top of the next page, and the achievable rate is $R_s = \log_2(1 + \gamma_s)$.

Note that for any given channel estimations $\hat{\mathbf{g}}_m$ and $\hat{\mathbf{h}}_m$, since the channel estimation errors $\tilde{\mathbf{g}}_m$ and $\tilde{\mathbf{h}}_m$ are random, the SINR in (36) and hence its rate R_s is random. By taking the expected achievable rate with respect to the random estimation

errors $\tilde{\mathbf{g}}_m$ and $\tilde{\mathbf{h}}_m$, we have the result (37) shown at the top of the next page, where we have denoted the average channel estimation-error-plus-noise power as

$$E = \sum_{m=1}^M P_m \left[\frac{b_m}{1 + e_1 b_m} + \frac{\alpha \epsilon_m (\frac{e_2 b_m}{1+e_1 b_m} + 1)}{\alpha e_2 \epsilon_m + \frac{e_2 b_m}{1+e_1 b_m} + 1} \right] + \sigma^2. \quad (38)$$

In (37), the lower bound of the expected primary communication rate $\mathbb{E}[R_s]$ is denoted by $\bar{R}_{s,\text{LB}}$. Note that the inequality in (37) follows from Jensen's inequality, and the fact that $\log_2(1 + C/x)$ is a convex function for $x > 0$.

Next, we derive the achievable rate of the secondary signals $c(n)$. After decoding $s(n)$, the primary signals $s(n)$ can be subtracted from (31) based on the estimated channel $\hat{\mathbf{g}}_m$. The resulting signal is

$$r_c(n) = \sum_{m=1}^M [\sqrt{\alpha} (\hat{\mathbf{h}}_m + \tilde{\mathbf{h}}_m)^H \mathbf{w}_m s(n) c(n) + \tilde{\mathbf{g}}_m^H \mathbf{w}_m s(n)] + z(n). \quad (39)$$

By treating the terms caused by the channel estimation error $\tilde{\mathbf{g}}_m$ and $\tilde{\mathbf{h}}_m$ as noise, (39) can be decomposed as

$$r_c(n) = \text{DS}'' \cdot c(n) + \text{ER} + z(n), \quad (40)$$

where ER accounts for the estimation errors given in (34), and DS'' denotes the desired signal in the decoding of the secondary signals $c(n)$, which is given by

$$\text{DS}'' = \sum_{m=1}^M \sqrt{\alpha} \hat{\mathbf{h}}_m^H \mathbf{w}_m s(n). \quad (41)$$

The resulting SINR is

$$\begin{aligned} \gamma_c &= \frac{|\text{DS}''|^2}{\mathbb{E}_{s(n), c(n)} [|\text{ER}|^2] + \sigma^2} \\ &= \frac{\alpha |\sum_{m=1}^M \hat{\mathbf{h}}_m^H \mathbf{w}_m|^2 |s(n)|^2}{\sum_{m=1}^M \sum_{l=1}^M \mathbf{w}_m^H (\tilde{\mathbf{g}}_m \tilde{\mathbf{g}}_l^H + \alpha \tilde{\mathbf{h}}_m \tilde{\mathbf{h}}_l^H) \mathbf{w}_l + \sigma^2}, \end{aligned} \quad (42)$$

and the achievable rate is $R_c = \log_2(1 + \gamma_c)$.

Note that different from (33), as the desired channel DS'' also depends on the primary symbols $s(n)$, the SINR in (42) is a random variable that depends on both $|s(n)|^2$ and the channel estimation errors. Consider the expectation of R_c , which is taken with respect to both $|s(n)|^2$ and the channel estimation errors, we have $\mathbb{E}[R_c]$ given in (43) at the top of next page. In (43) the inequality is obtained by applying Jensen's inequality to the convex function $\log_2(1 + C/x)$, and $\beta'_c = \frac{\alpha |\sum_{m=1}^M \hat{\mathbf{h}}_m^H \mathbf{w}_m|^2}{E}$ represents the average SINR for the secondary signals taking into account the channel estimation errors. Similarly, we denote the lower bound of expectation rate $\mathbb{E}[R_c]$ with $\bar{R}_{c,\text{LB}}$.

D. Rate-Region Characterization with Imperfect CSI

In this subsection, the achievable rate-region of cell-free symbiotic radio system is characterized by taking into account the CSI estimation errors.

Similar to the optimization problem (6) with perfect CSI studied in Section III, the achievable rate-region under channel estimation errors can be characterized by maximizing the expected secondary communication rate $\bar{R}_{c,\text{LB}}$ in (43) with

$$\begin{aligned}
\gamma_s &= \frac{|\text{DS}'|^2}{\mathbb{E}_{s(n),c(n)}[|\text{ER}|^2] + \mathbb{E}_{s(n),c(n)}[|\text{ST}|^2] + \sigma^2} \\
&= \frac{|\sum_{m=1}^M \hat{\mathbf{g}}_m^H \mathbf{w}_m|^2}{\mathbb{E}_{s(n),c(n)}[|s(n)|^2 |\sum_{m=1}^M (\tilde{\mathbf{g}}_m + \sqrt{\alpha} \tilde{\mathbf{h}}_m c(n))^H \mathbf{w}_m|^2] + \alpha \mathbb{E}_{s(n),c(n)}[|\sum_{m=1}^M \hat{\mathbf{h}}_m^H \mathbf{w}_m|^2 |s(n)|^2 |c(n)|^2] + \sigma^2} \\
&= \frac{|\sum_{m=1}^M \hat{\mathbf{g}}_m^H \mathbf{w}_m|^2}{\sum_{m=1}^M \sum_{l=1}^M \mathbf{w}_m^H (\tilde{\mathbf{g}}_m \tilde{\mathbf{g}}_l^H + \alpha \tilde{\mathbf{h}}_m \tilde{\mathbf{h}}_l^H) \mathbf{w}_l + \alpha |\sum_{m=1}^M \hat{\mathbf{h}}_m^H \mathbf{w}_m|^2 + \sigma^2}.
\end{aligned} \tag{36}$$

$$\begin{aligned}
\mathbb{E}[R_s] &= \mathbb{E}_{\tilde{\mathbf{g}}_m, \tilde{\mathbf{h}}_m} [\log_2(1 + \gamma_s)] \\
&\geq \log_2 \left(1 + \frac{|\sum_{m=1}^M \hat{\mathbf{g}}_m^H \mathbf{w}_m|^2}{\mathbb{E}_{\tilde{\mathbf{g}}_m, \tilde{\mathbf{h}}_m} [\sum_{m=1}^M \sum_{l=1}^M \mathbf{w}_m^H (\tilde{\mathbf{g}}_m \tilde{\mathbf{g}}_l^H + \alpha \tilde{\mathbf{h}}_m \tilde{\mathbf{h}}_l^H) \mathbf{w}_l] + \alpha |\sum_{m=1}^M \hat{\mathbf{h}}_m^H \mathbf{w}_m|^2 + \sigma^2} \right) \\
&= \log_2 \left(1 + \frac{|\sum_{m=1}^M \hat{\mathbf{g}}_m^H \mathbf{w}_m|^2}{\sum_{m=1}^M \mathbf{w}_m^H (\mathbf{R}_{\tilde{\mathbf{g}},m} + \alpha \mathbf{R}_{\tilde{\mathbf{h}},m}) \mathbf{w}_m + \sigma^2 + \alpha |\sum_{m=1}^M \hat{\mathbf{h}}_m^H \mathbf{w}_m|^2} \right) \\
&= \log_2 \left(1 + \frac{|\sum_{m=1}^M \hat{\mathbf{g}}_m^H \mathbf{w}_m|^2}{E + \alpha |\sum_{m=1}^M \hat{\mathbf{h}}_m^H \mathbf{w}_m|^2} \right) \\
&\triangleq \bar{R}_{s,\text{LB}}.
\end{aligned} \tag{37}$$

$$\begin{aligned}
\mathbb{E}[R_c] &= \mathbb{E}_{\tilde{\mathbf{g}}_m, \tilde{\mathbf{h}}_m, s(n)} [\log_2(1 + \gamma_c)] \geq \mathbb{E}_{s(n)} \left[\log_2 \left(1 + \frac{\alpha |\sum_{m=1}^M \hat{\mathbf{h}}_m^H \mathbf{w}_m|^2 |s(n)|^2}{\mathbb{E}_{\tilde{\mathbf{g}}_m, \tilde{\mathbf{h}}_m} [\sum_{m=1}^M \sum_{l=1}^M \mathbf{w}_m^H (\tilde{\mathbf{g}}_m \tilde{\mathbf{g}}_l^H + \alpha \tilde{\mathbf{h}}_m \tilde{\mathbf{h}}_l^H) \mathbf{w}_l] + \sigma^2} \right) \right] \\
&= \mathbb{E}_{s(n)} \left[\log_2 \left(1 + \frac{\alpha |\sum_{m=1}^M \hat{\mathbf{h}}_m^H \mathbf{w}_m|^2 |s(n)|^2}{E} \right) \right] = \int_0^\infty \log_2(1 + \beta'_c x) e^{-x} dx \\
&= -e^{\frac{1}{\beta'_c}} \text{Ei} \left(-\frac{1}{\beta'_c} \right) \log_2 e \\
&\triangleq \bar{R}_{c,\text{LB}}.
\end{aligned} \tag{43}$$

a given targeting primary communication rate constraint R_{th} for $\bar{R}_{s,\text{LB}}$ in (37). The optimization problem can be formulated as

$$\max_{\mathbf{w}_m, m=1, \dots, M} \bar{R}_{c,\text{LB}} \tag{44a}$$

$$\text{s.t. } \bar{R}_{s,\text{LB}} \geq R_{\text{th}}, \tag{44b}$$

$$\|\mathbf{w}_m\|^2 \leq P_m, \quad m = 1, \dots, M. \tag{44c}$$

Since the $\bar{R}_{c,\text{LB}}$ is also monotonically increasing with respect to β'_c , the objective function (44a) is equivalent to β'_c . Therefore, problem (44) can be equivalently written as

$$\max_{\mathbf{w}_m, m=1, \dots, M} \left| \sum_{m=1}^M \hat{\mathbf{h}}_m^H \mathbf{w}_m \right|^2, \tag{45a}$$

$$\text{s.t. } \log_2 \left(1 + \frac{|\sum_{m=1}^M \hat{\mathbf{g}}_m^H \mathbf{w}_m|^2}{E + \alpha |\sum_{m=1}^M \hat{\mathbf{h}}_m^H \mathbf{w}_m|^2} \right) \geq R_{\text{th}}, \tag{45b}$$

$$\|\mathbf{w}_m\|^2 \leq P_m, \quad m = 1, \dots, M. \tag{45c}$$

Note that different from problem (7) that requires perfect CSI, problem (45) only requires the estimated channel CSI $\hat{\mathbf{g}}_m^H$ and $\hat{\mathbf{h}}_m^H$, $m = 1, \dots, M$, and the impact of CSI estimation error is reflected in E . Furthermore, since problem (45) has

exactly the same structure as (7), the feasibility analysis as well as the proposed solution in Theorem 1 and Algorithm 2 can be directly used to solve problem (45). The details are omitted to avoid repetition.

V. SIMULATION RESULTS

In this section, simulation results are provided to evaluate the performance of our proposed design for cell-free symbiotic radio systems. Without loss of generality, we establish a Cartesian coordinate system, where the BD is located at the origin (0,0), and the receiver is located at (5m, 0). Furthermore, $M = 16$ APs, each with $N = 4$ antennas, are evenly spaced in a square area of size 750m \times 750m, i.e., their locations correspond to the 4×4 grid points, with the x- and y-coordinates chosen from the set $\{-375\text{m}, -125\text{m}, 125\text{m}, 375\text{m}\}$. The small-scale fading coefficients for the channels of different communication links follow the i.i.d. CSCG distribution with zero mean and unit variance. Furthermore, the large-scale channel gains of AP-to-BD and AP-to-receiver links are modeled as $b_m = \beta_0 d_m^{-\gamma}$, where $\beta_0 = (\frac{\lambda}{4\pi})^2$ is the reference channel gain, with $\lambda = 0.0857\text{m}$ denoting the wavelength, d_m represents the corresponding channel link distance of AP-to-BD or AP-to-receiver, and γ denotes the path loss exponent. We set $\gamma = 2.7$ for the AP-to-BD and AP-to-receiver channels.

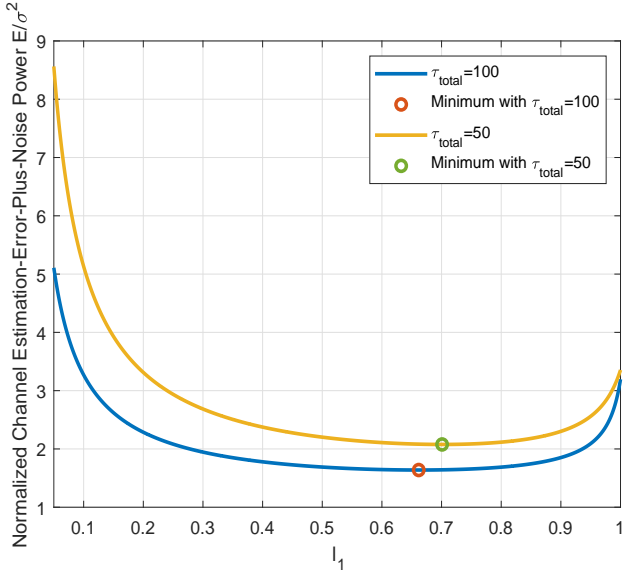


Fig. 2. Normalized channel estimation-error-plus-noise power E/σ^2 versus primary pilot length ratio l_1 in phase 1.

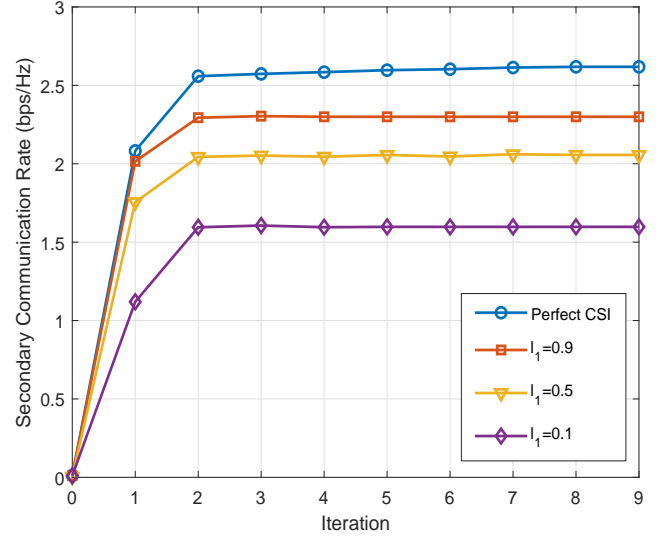


Fig. 4. Convergence of the SCA iteration process with different primary pilot length ratio l_1 , where $R_{th} = 12\text{bps/Hz}$, $\tau_{total} = 100$.

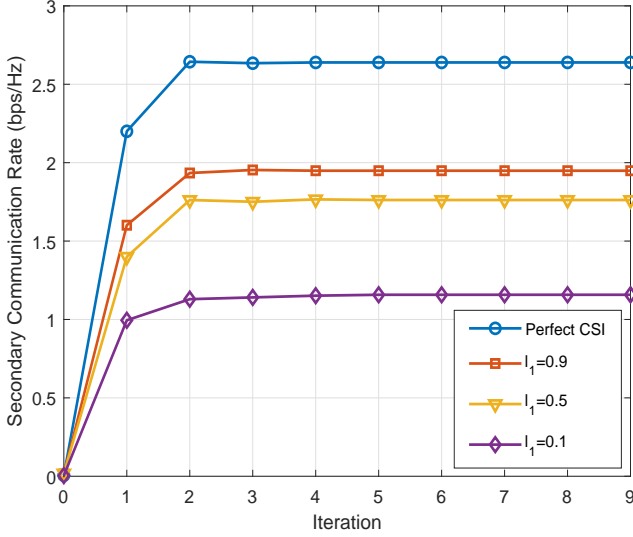


Fig. 3. Convergence of the SCA iteration process with different primary pilot length ratio l_1 , where $R_{th} = 12\text{bps/Hz}$, $\tau_{total} = 50$.

And the large-scale channel coefficients ϵ_m of the cascaded AP-BD-receiver channels are modeled as $\epsilon_m = 0.001\zeta_m$, where ζ_m represents the large-scale coefficients of AP-to-BD channels. The power reflection coefficient is $\alpha = 1$, and the transmitter-side SNR for data and pilot transmission are set as $\frac{P_m}{\sigma^2} = \frac{P_t}{\sigma^2} = 130\text{ dB}$, $m = 1, \dots, M$, which may correspond to $P_m = P_t = 20\text{ dBm}$ and $\sigma^2 = -110\text{ dBm}$. The termination threshold for Algorithm 1 is set as $\kappa_1 = 0.5\%$. We further denote $\tau_{total} = \tau_1 + \tau_2$ as the total pilot length used for channel estimation in phase 1 and phase 2 and $l_1 = \frac{\tau_1}{\tau_{total}}$ and $l_2 = \frac{\tau_2}{\tau_{total}}$ denote the ratios of the total pilot length allocated for the first and second training phases, respectively.

A. Channel Estimation Error and Convergence of SCA Algorithm

As can be inferred from (37) and (43), with imperfect CSI, not only the additive noise but also the channel estimation error will impair the performance of cell-free symbiotic radio systems. Therefore, Fig. 2 shows the normalized channel estimation-error-plus-noise power, i.e., E/σ^2 , where E is given in equation (38) and the normalization is taken with respect to the noise power σ^2 . The ratio l_1 of the training phase 1 varies from 0.05 to 1. The total pilot length τ_{total} is set as 50 and 100, respectively. Note that with perfect CSI, we have $\frac{E}{\sigma^2} = 1$. It is observed from Fig. 2 that the curve with $\tau_{total} = 100$ always stays below the curve with $\tau_{total} = 50$. This is expected since the accuracy of channel estimation can be improved with a longer pilot length. Furthermore, for both $\tau_{total} = 100$ and $\tau_{total} = 50$, as ratio l_1 increases, E/σ^2 first decreases, and then increases slowly after reaching their lowest point. This is expected since for a given total training length, there exists a trade-off between the estimation error in phase 1 and phase 2, as can be inferred from (38). Specifically, the increase of l_1 increases the training ENR e_1 , which effectively reduces the primary channel estimation error in (23), while the secondary cascaded channels suffer from more serious estimation error. Besides, it can be inferred from Fig. 2 that the average channel estimation-error-plus-noise power E is more sensitive to the pilot length of phase 1 than that of phase 2. Specifically, when a short pilot was allocated to phase 1 (say $l_1 = 0.1$), the corresponding E/σ^2 is much higher than its counterpart with $l_1 = 0.9$, which corresponds a low pilot allocation to phase 2. This is expected since the estimation error of the primary channels in phase 1 also affects the channel estimation accuracy of the secondary cascaded link in phase 2, as can be inferred from (30). As a result, with a limited pilot length, higher priority should be given to phase 1 in order to decrease the estimation error of the whole system. Fig. 2 also

labels the optimal pilot allocation for which E/σ^2 achieves the minimum value. It is observed that around the optimal point, the curves are rather flat, indicating that the impact of the channel estimation error would be comparable for a wide range of pilot length allocations, say for $0.3 < l_1 < 0.9$. Therefore, in the following, we choose $l_1 = 0.1, 0.5, 0.9$ as the representative values to show the impact of different pilot length allocations on system performance.

Fig. 3 and Fig. 4 show the convergence of the proposed SCA based algorithm in Algorithm 2 with total pilot lengths of $\tau_{\text{total}} = 50$ and 100, respectively. The iterations start with randomly generated initial local points, with a rate threshold of $R_{\text{th}} = 12$ bps/Hz and an iteration terminating threshold of $\kappa_2 = 0.5\%$. Note that different curves in Fig. 3 and Fig. 4 show the convergence with perfect CSI and different primary pilot length ratios l_1 , respectively. As shown in the figure, the passive secondary communication rate, which is the optimization objective of problem (7), increases monotonically during iterations, which is in accordance with Lemma 1. Furthermore, Fig. 3 and Fig. 4 show that only a few iterations are needed for Algorithm 2 to converge.

B. Achievable Rate-Region

Fig. 5 shows the achievable rate-region of the primary and secondary communication rates with perfect and imperfect CSI, respectively. In the case of imperfect CSI, the primary pilot length ratios are selected as $l_1 = 0.1, 0.5, 0.9$, and the simulation results are obtained by running 500 experiments at each primary pilot length ratio based on the random cell-free symbiotic radio system channel realization. The total pilot length τ_{total} is set to 50. Note that each point of the curve corresponds to a primary-secondary rate pair, by varying the primary communication threshold R_{th} from \hat{R}_s to \bar{R}_s with step size 1. Meanwhile, the dot-dash line shows the portion with $R_{\text{th}} \leq \hat{R}_s$, where the optimization problem has a closed-form solution given in Theorem 1, and the primary and secondary communication rate can be obtained in (11) and (14). If $\hat{R}_s < R_{\text{th}} \leq \bar{R}_s$, the achievable rate of the secondary backscattering communication decreases monotonically as the primary communication threshold R_{th} increases, and eventually approaching zero. It is observed from Fig. 5 that with the total pilot length τ_{total} fixed, the achievable rate-region taking into account imperfect CSI estimation, is highly dependent on the allocation of the pilot l_1 . Out of the three pilot allocation considered, $l_1 = 0.5$ gives the best performance. This is consistent with Fig. 2, where $l_1 = 0.5$ gives smaller channel estimation error than $l_1 = 0.1$ and $l_1 = 0.9$. Furthermore, Fig. 5 also shows that $l_1 = 0.9$ outperforms $l_1 = 0.1$. This is also consistent with Fig. 2, by comparing their respective channel estimation errors.

Fig. 6 shows the achievable rate-region with a fixed total pilot length $\tau_{\text{total}} = 100$. Similar to Fig. 5, a higher primary communication threshold R_{th} brings a lower secondary communication rate. Besides, when comparing Fig. 6 to Fig. 5, it is observed that larger rate-region is achieved for any given pilot allocation l_1 in Fig. 6 than its counterpart in Fig. 5. This is expected since a longer pilot length enhances the

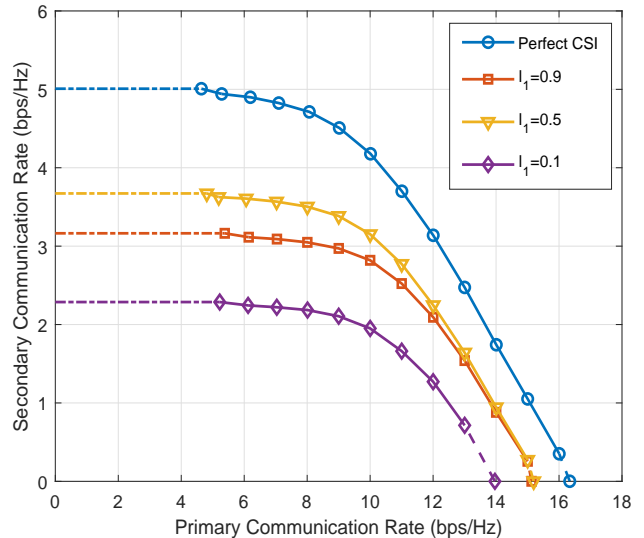


Fig. 5. The achievable rate-region of cell-free symbiotic radio system, where $\tau_{\text{total}} = 50$.

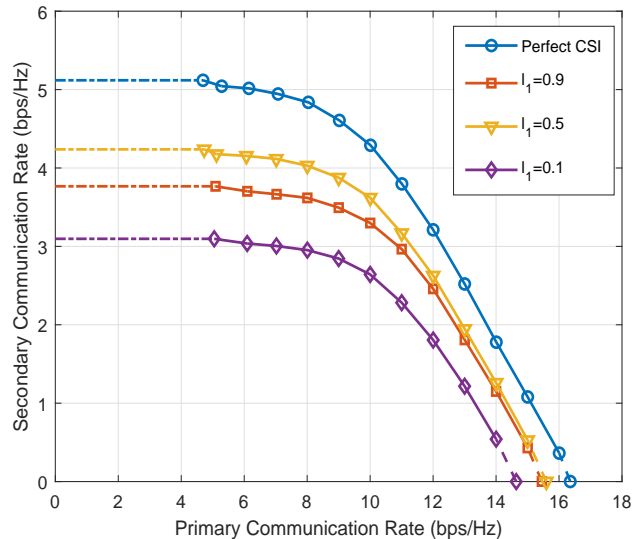


Fig. 6. The achievable rate-region of cell-free symbiotic radio system, where $\tau_{\text{total}} = 100$.

estimation accuracy of both the active primary and passive secondary channels, thus enlarging the achievable rate-region significantly. Meanwhile, it is observed that the performance gap between $l_1 = 0.5$ and $l_1 = 0.9$ is smaller in Fig. 5 than that in Fig. 6, while the reverse is true for the gap between $l_1 = 0.5$ and $l_1 = 0.1$. This implies that the performance improvement to increase the priority for primary channel estimation is more significant when τ_{total} is relatively small. Thus, when the pilot length τ_{total} is severely limited, higher priority should be given to the training phase 1. This is expected since the estimation of the direct-link channels in the first phase affects not only the primary communication rate, but also the quality of the channel estimation of the backscatter channels.

VI. CONCLUSION

In this paper, a novel cell-free symbiotic radio system was investigated, in which a number of distributed APs cooperatively send primary information to the receiver, while concurrently supporting the secondary backscattering communication. The achievable rates of both the active primary and passive secondary communications were first derived under the assumption of perfect CSI. Furthermore, a two-phase uplink-training based channel estimation method was proposed to effectively estimate the direct-link channel and cascaded backscatter channel, and the achievable rates were revisited with channel estimation errors. In order to characterize the achievable rate-region, a beamforming optimization problem was formulated to maximize the passive secondary communication rate with a targeting active primary communication rate constraint, for both perfect CSI and imperfect CSI. Efficient algorithms were proposed to solve the formulated optimization problem. The performance of the cell-free symbiotic radio communication systems was validated with extensive simulation results.

APPENDIX A PROOF OF THEOREM 1

To prove Theorem 1, we first consider a relaxed problem of (7) by omitting the targeting primary communication rate constraint (7b). The problem is formulated as

$$\max_{\mathbf{w}_m, m=1, \dots, M} \left| \sum_{m=1}^M \mathbf{f}_m^H \mathbf{w}_m \right|^2 \quad (46a)$$

$$\text{s.t.} \quad \|\mathbf{w}_m\|^2 \leq P_m, \quad m = 1, \dots, M. \quad (46b)$$

It is not difficult to see that the optimal solution to problem (46) is the per-AP maximum ratio transmission (MRT) beamforming with maximum transmit power, which is given by (12) in Theorem 1. In this case, the corresponding primary communication rate on the left hand side of (7b) is given in \widehat{R}_s shown in (11).

Therefore, when the condition $R_{\text{th}} \leq \widehat{R}_s$ given in Theorem 1 is satisfied, the solution in (12) satisfies both constraints in (7b) and (7c), and thus it is also feasible to the original problem (7). Furthermore, since the beamforming vectors in (12) is the optimal solution to the relaxed problem (46) and is also feasible to (7), it must also be the optimal solution to the original problem (7), since the former has a larger feasibility region than the latter.

This completes the proof of Theorem 1.

APPENDIX B PROOF OF LEMMA 1

To prove Lemma 1, we note that at the $(l+1)$ -th iteration, with Step 4 of Algorithm 2, we have $\mathbf{w}^{(l+1)} = \mathbf{w}^{*(l)}$, where $\mathbf{w}^{*(l)}$ represents the optimal solution at the (l) -th iteration.

Therefore, the lower bound (16) holds with equality at the local point $\mathbf{w} = \mathbf{w}^{*(l)}$, i.e.,

$$\begin{aligned} F(\mathbf{w}^{*(l)}) &= |\mathbf{f}^H \mathbf{w}^{*(l)}|^2 = F_{\text{low}}(\mathbf{w}^{*(l)} | \mathbf{w}^{*(l)}) \\ &= F_{\text{low}}(\mathbf{w}^{*(l)} | \mathbf{w}^{(l+1)}), \forall l. \end{aligned} \quad (47)$$

Furthermore, with (16) and Algorithm 2, we obtain the following relationship

$$\begin{aligned} F(\mathbf{w}^{*(l+1)}) &\stackrel{(a)}{\geq} F_{\text{low}}(\mathbf{w}^{*(l+1)} | \mathbf{w}^{(l+1)}) \\ &\stackrel{(b)}{\geq} F_{\text{low}}(\mathbf{w}^{*(l)} | \mathbf{w}^{(l+1)}) \stackrel{(c)}{=} F(\mathbf{w}^{*(l)}), \end{aligned} \quad (48)$$

where the inequality (a) follows from the global lower bound (16), the inequality (b) holds since $\mathbf{w}^{*(l+1)}$ is the optimal solution of problem (17) in the $(l+1)$ -th iteration, and the equality (c) follows from (47).

Thus, the relationship (48) shows that the objective value $F(\mathbf{w}^{*(l)})$ of (15) obtained in Algorithm 2 is monotonically non-decreasing, and hence converges to a finite limit. Besides, note that the lower bound $F_{\text{low}}(\mathbf{w} | \mathbf{w}^{(l+1)})$ has identical gradient as $F(\mathbf{w})$ at the local point $\mathbf{w}^{*(l)}$, i.e.,

$$\nabla F(\mathbf{w}^{*(l)}) = \nabla F_{\text{low}}(\mathbf{w}^{*(l)} | \mathbf{w}^{(l+1)}). \quad (49)$$

Then the sequence $\mathbf{w}^{*(l)}$ converges to a point that fulfills the KKT optimality conditions of the original non-convex problem (15) [33]–[35].

This completes the proof of Lemma 1.

REFERENCES

- [1] M. Latva-aho and K. L. (eds.), "Key drivers and research challenges for 6G ubiquitous wireless intelligence," *6G Research Visions 1, 6G Flagship*, University of Oulu, Finland, Sep. 2019.
- [2] X. You et al., "Towards 6G wireless communication networks: vision, enabling technologies, and new paradigm shifts," *Sci. China Inf. Sci.*, vol. 64, no. 1, pp. 1–74, Nov. 2020.
- [3] Y. Zeng and X. Xu, "Toward environment-aware 6g communications via channel knowledge map," *IEEE Wirel. Commun.*, vol. 28, no. 3, pp. 84–91, Jun. 2021.
- [4] S. Hu, F. Rusek, and O. Edfors, "Beyond massive MIMO: The potential of data transmission with large intelligent surfaces," *IEEE Trans. Signal Process.*, vol. 66, no. 10, pp. 2746–2758, Mar. 2018.
- [5] H. Lu and Y. Zeng, "Communicating with extremely large-scale array/surface: unified modelling and performance analysis," *IEEE Trans. Wirel. Commun.*, Early Access, DOI:10.1109/TWC.2021.3126384
- [6] M. R. Akdeniz, Y. Liu, M. K. Samimi, S. Sun, S. Rangan, T. S. Rappaport, and E. Erkip, "Millimeter wave channel modeling and cellular capacity evaluation," *IEEE J. Sel. Areas Commun.*, vol. 32, no. 6, pp. 1164–1179, Jun. 2014.
- [7] H. Elayan, O. Amin, R. M. Shubair, and M.-S. Alouini, "Terahertz communication: The opportunities of wireless technology beyond 5G," in *Proc. IEEE Int. Conf. Adv. Commun. Technol. Netw.(CommNet)*, Apr. 2018, pp. 1–5.
- [8] M. Giordani and M. Zorzi, "Non-terrestrial networks in the 6G era: Challenges and opportunities," *IEEE Netw.*, vol. 35, no. 2, pp. 244–251, Dec. 2021.
- [9] Y. Zeng, Q. Wu, and R. Zhang, "Accessing from the sky: A tutorial on UAV communications for 5G and beyond," *Proc. IEEE*, vol. 107, no. 12, pp. 2327–2375, Dec. 2019.
- [10] W. Tang, X. Li, J. Y. Dai, S. Jin, Y. Zeng, Q. Cheng, and T. J. Cui, "Wireless communications with programmable metasurface: Transceiver design and experimental results," *China Commun.*, vol. 16, no. 5, pp. 46–61, Jun. 2019.

- [11] Q. Wu, S. Zhang, B. Zheng, C. You, and R. Zhang, "Intelligent reflecting surface-aided wireless communications: A tutorial," *IEEE Trans. Wirel. Commun.*, vol. 69, no. 5, pp. 3313–3351, May. 2021.
- [12] N. C. Luong, D. T. Hoang, S. Gong, D. Niyato, P. Wang, Y.-C. Liang, and D. I. Kim, "Applications of deep reinforcement learning in communications and networking: A survey," *IEEE Commun. Surv. Tutor.*, vol. 21, no. 4, pp. 3133–3174, May. 2019.
- [13] H. Q. Ngo, A. Ashikhmin, H. Yang, E. G. Larsson, and T. L. Marzetta, "Cell-free massive MIMO versus small cells," *IEEE Trans. Wirel. Commun.*, vol. 16, no. 3, pp. 1834–1850, Jan. 2017.
- [14] Y.-C. Liang, Q. Zhang, E. G. Larsson, and G. Y. Li, "Symbiotic radio: Cognitive backscattering communications for future wireless networks," *IEEE Trans. Cogn. Commun. Netw.*, vol. 6, no. 4, pp. 1242–1255, Sep. 2020.
- [15] Z. Dai, R. Li, J. Xu, Y. Zeng, and S. Jin, "Cell-free symbiotic radio: Channel estimation method and achievable rate analysis," in *Proc. 2021 IEEE/CIC ICCO Workshops*, 2021, pp. 25–30.
- [16] E. Björnson and L. Sanguinetti, "Scalable cell-free massive mimo systems," *IEEE Trans. Commun.*, vol. 68, no. 7, pp. 4247–4261, Jul. 2020.
- [17] Z. Chen and E. Björnson, "Channel hardening and favorable propagation in cell-free massive MIMO with stochastic geometry," *IEEE Trans. Commun.*, vol. 66, no. 11, pp. 5205–5219, Nov. 2018.
- [18] G. Interdonato, E. Björnson, H. Q. Ngo, P. Frenger, and E. G. Larsson, "Ubiquitous cell-free massive MIMO communications," *EURASIP J. Wireless Commun. Netw.*, pp. 1–19, Aug. 2019.
- [19] E. Nayebi, A. Ashikhmin, T. L. Marzetta, H. Yang, and B. D. Rao, "Precoding and power optimization in cell-free massive MIMO systems," *IEEE Trans. Wirel. Commun.*, vol. 16, no. 7, pp. 4445–4459, May. 2017.
- [20] M. Bashar, K. Cumanan, A. G. Burr, M. Debbah, and H. Q. Ngo, "On the uplink max-min sinr of cell-free massive mimo systems," *IEEE Trans. Wirel. Commun.*, vol. 18, no. 4, pp. 2021–2036, Apr. 2019.
- [21] M. Bashar, K. Cumanan, A. G. Burr, H. Q. Ngo, L. Hanzo, and P. Xiao, "On the performance of cell-free massive mimo relying on adaptive NOMA/OMA mode-switching," *IEEE Trans. Commun.*, vol. 68, no. 2, pp. 792–810, Feb. 2020.
- [22] L. D. Nguyen, T. Q. Duong, H. Q. Ngo, and K. Tourki, "Energy efficiency in cell-free massive MIMO with zero-forcing precoding design," *IEEE Commun. Lett.*, vol. 21, no. 8, pp. 1871–1874, Apr. 2017.
- [23] H. Q. Ngo, L.-N. Tran, T. Q. Duong, M. Matthaiou, and E. G. Larsson, "On the total energy efficiency of cell-free massive MIMO," *IEEE Trans. Green Commun. Netw.*, vol. 2, no. 1, pp. 25–39, Nov. 2018.
- [24] R. Long, Y.-C. Liang, H. Guo, G. Yang, and R. Zhang, "Symbiotic radio: A new communication paradigm for passive internet of things," *IEEE Internet Things J.*, vol. 7, no. 2, pp. 1350–1363, Nov. 2020.
- [25] R. Long, H. Guo, L. Zhang, and Y.-C. Liang, "Full-duplex backscatter communications in symbiotic radio systems," *IEEE Access*, vol. 7, pp. 21 597–21 608, Feb. 2019.
- [26] H. Guo, Y.-C. Liang, R. Long, and Q. Zhang, "Cooperative ambient backscatter system: A symbiotic radio paradigm for passive IoT," *IEEE Wirel. Commun. Lett.*, vol. 8, no. 4, pp. 1191–1194, Apr. 2019.
- [27] T. Wu, M. Jiang, Q. Zhang, Q. Li, and J. Qin, "Beamforming design in multiple-input-multiple-output symbiotic radio backscatter systems," *IEEE Commun. Lett.*, pp. 1–1, Feb. 2021.
- [28] H. Guo, Y.-C. Liang, R. Long, S. Xiao, and Q. Zhang, "Resource allocation for symbiotic radio system with fading channels," *IEEE Access*, vol. 7, pp. 34 333–34 347, Mar. 2019.
- [29] Z. Chu, W. Hao, P. Xiao, M. Khalily, and R. Tafazolli, "Resource allocations for symbiotic radio with finite blocklength backscatter link," *IEEE Internet Things J.*, vol. 7, no. 9, pp. 8192–8207, Mar. 2020.
- [30] D. Mishra and E. G. Larsson, "Optimal channel estimation for reciprocity-based backscattering with a full-duplex mimo reader," *IEEE Trans. Signal Process.*, vol. 67, no. 6, pp. 1662–1677, Mar. 2019.
- [31] F. Kaltenberger, H. Jiang, M. Guillaud, and R. Knopp, "Relative channel reciprocity calibration in MIMO/TDD systems," in *Proc. Future Network and Mobile Summit*, Florence, Italy, Jun. 2010, pp. 1–10.
- [32] T. L. Marzetta, "Noncooperative cellular wireless with unlimited numbers of base station antennas," *IEEE Trans. Wirel. Commun.*, vol. 9, no. 11, pp. 3590–3600, Oct. 2010.
- [33] Y. Zeng and R. Zhang, "Energy-efficient UAV communication with trajectory optimization," *IEEE Trans. Wirel. Commun.*, vol. 16, no. 6, pp. 3747–3760, Jun. 2017.
- [34] A. Zappone, E. Björnson, L. Sanguinetti, and E. Jorswieck, "Globally optimal energy-efficient power control and receiver design in wireless networks," *IEEE Trans. Signal Process.*, vol. 65, no. 11, pp. 2844–2859, Jun. 2017.
- [35] B. R. Marks and G. P. Wright, "A general inner approximation algorithm for non-convex mathematical programs," *Oper. Res.*, vol. 26, no. 4, pp. 681–683, Jan. 1978.
- [36] F. Neeser and J. Massey, "Proper complex random processes with applications to information theory," *IEEE Trans. Inf. Theory*, vol. 39, no. 4, pp. 1293–1302, Jul. 1993.
- [37] B. Hassibi and B. Hochwald, "How much training is needed in multiple-antenna wireless links?" *IEEE Trans. Inf. Theory*, vol. 49, no. 4, pp. 951–963, Apr. 2003.
- [38] Q. Zhang, L. Zhang, Y.-C. Liang, and P.-Y. Kam, "Backscatter-noma: A symbiotic system of cellular and Internet-of-Things networks," *IEEE Access*, vol. 7, pp. 20 000–20 013, Feb. 2019.
- [39] D. Tse and P. Viswanath, *Fundamentals of Wireless Communication*. Cambridge, U.K.: Cambridge Univ. Press, 2005.
- [40] M. Grant and S. Boyd. (2008). *CVX: Matlab Software for Disciplined Convex Programming*. [Online]. Available: <http://cvxr.com/cvx>
- [41] A. Hjørungnes, *Complex-valued matrix derivatives: with applications in signal processing and communications*. Cambridge University Press, 2011.
- [42] S. Boyd and L. Vandenberghe, *Convex Optimization*. Cambridge, U.K.: Cambridge Univ, 2005.
- [43] S. K. Sengupta, "Fundamentals of statistical signal processing: Estimation theory," Oxford, U.K.: Taylor & Francis, 1995.
- [44] Y. Zeng, R. Zhang, and Z. N. Chen, "Electromagnetic lens-focusing antenna enabled massive MIMO: Performance improvement and cost reduction," *IEEE J. Sel. Areas Commun.*, vol. 32, no. 6, pp. 1194–1206, Jun. 2014.